Chapter

Multi-Field Synergy Process for Polymer Plasticization: A Novel Design Concept for Screw to Facilitate Phase-to-Phase Thermal and Molecular Mobility

Ranran Jian, Hongbo Chen and Weimin Yang

Abstract

A novel concept of screw design has been proposed considering the multi-field synergy principle to facilitate phase-to-phase thermal and molecular mobility; subsequently, a torsion element has been designed. This new screw design allows an innovative and effective way to resolve a growing challenge in polymer process engineering, especially for nanocomposites or biopolymers, that is, an inadequate control of mass transfer and thermal management for multicomponent melt flows through narrow channels during extrusion or injection. The adaption of torsion element in the screw facilitated the plasticization mixing and thermal distribution in polymer melts, and the torsional flow induced by the torsion elements shows a synergistic effect on the melt-phase mass flow and the thermal flow field. The latter effect enhances the mass and heat transfer of heterogeneous polymer systems and realizes effective heat management to achieve properly uniform temperature field.

Keywords: multi-field coupling, polymer plasticization, field synergy, torsional flow, heat and mass transfer enhancement

1. Introduction

Polymer plasticization is a complex process with many uncertain variables, which involves phase transfer and viscoelastic behavior. The nonlinear effect of polymer plasticization is a multidisciplinary engineering science problem that includes heat transfer, rheology, and flow dynamics among others. The thermal homogeneity and stability of polymer melts in this plasticization process is the key to determine the quality of products, especially for biodegradable nanocomposites or microcellular foam materials.

In polymer processing, plasticization screw is an added unit operation that facilitates melting and homogenization of an initially heterogeneous physical system [1, 2]. In general, the temperature distribution is not uniform in the process of plasticization; this is due to significant friction heating and the low thermal conductivity of polymers. It is very important to optimize the structural parameters and working characteristics of the screw in order to enhance plasticization of

polymers. The effect of barrel configurations and screw designs on heat and mass transfer has been investigated in the past and proved unquestionably important attributes for determining temperature uniformity and mixing effectiveness in extrusion and injection molding processes [3–8]. Different from conventional screw, the new types of screw can be roughly divided into four categories: distribution screws, barrier screws, separator screws, and channel screws with variable sections. These reconfigured screws are stated to be better than a standard one. For example, Kelly et al. [6] developed a barrier-flighted screw with Maddock mixer to achieve good melting performance and low temperature and pressure fluctuations. Spalding [9] introduced a distributive melt-mixing type screw equipped with an Eagle mixer in injection molding process and obtained better melting capacity and higher mixing than a conventional screw. Shimbo et al. [10] disclosed a mixture system by combining Pin and Dulmage type screws and also reported their beneficial effect in kneading, homogenization, and ensuring stability of gas/polymer solution. Zitzenbacher et al. [11, 12] indicated that the shearing sections like axial and spiral Maddock elements and Z-elements are often used to improve the melt homogeneity by enhancing dispersive mixing. Rydzkowski [13] developed an autothermal screw-disc extruder to induce autothermal effect. Rauwendaal [4] noted a CRD mixing screw with wedge-shaped barrier region to generate elongational flow. In this way, the mixing ability improves under the condition of lower power consumption and viscous dissipation than shear flow. Also, the melt temperatures and pressure fluctuation reduce in the flow channel. Based on the elongational flow and volume transportation, Qu et al. [14, 15] proposed a novel vane plasticization system in place of screw one to create extensional stress. Their results showed that the plasticizing capacity improved with the decrease of power consumption in the vane extruder. Diekmann [16] analyzed the direct-drive single-screw extruders without gearing and results indicated that plasticization capacity increased in the direct-drive system. Besides, Jiang [17] introduced ultrasonic plasticizing in the extruder to achieve energy saving. And Qu et al. [18] introduced a vibrational force field in the screw plasticization system. Their results showed that mixing performance improved and extrusion pressure reduced.

These studies may focus on mixing and rheology. However, heat transfer also plays a significant role in plasticizing. In the past, researchers paid little attention to understand heat transfer in viscous fluid. Understanding the mass and heat transfer processes in a plasticization system as a function of screw configurations is essential to further develop a more effective screw design to overcome some of the existing challenges. The properties of composites in the plasticization process also depend on the control of the velocity, temperature, shear, and pressure fields. Therefore, it is worth investigating the synergetic relationship, if any, between various physical fields in order to maximize the efficiency of the plasticization effect.

Mixing a high-viscosity or high-molecular weight polymer melt leads to shear-induced overheating due to the large torque induced, required to unleash the polymer chain entanglements. The challenge in this case is to fabricate a screw configuration that facilitates polymer chain mobility in melt phase without inducing high shear and by facilitating effective transfer of the excess local heat out of the bulk of the polymer melt. Otherwise, the local overheating effect essentially results in unwanted heat loss and poor melt quality, subsequently, the polymer chains break down and thermosensitive polymers such as biopolymers may even be degraded.

In order to overcome the challenges of an inadequate control of flow-thermal management for multicomponent melt, we explore the synergistic relationship and interaction mechanism between various physical fields for non-Newtonian viscous liquids such as polymer melts, with special emphasis on higher molecular weight thermoplastic resins, subsequently a torsion screw has been designed.

2. Multi-field synergy theory

In order to find out relationships among the velocity, velocity gradient, and temperature gradient fields in the plasticization process of polymer, we presented the mathematical expressions for quantitative analysis of multi-field synergy based on momentum conservation equation and energy conservation equation.

2.1 Synergy between velocity and velocity gradient

From the knowledge of polymer rheology, we have obtained the Navier-Stokes equation derived from momentum conservation equation in the form of Eq. (1).

$$\rho \frac{\mathrm{D}\vec{v}}{\mathrm{D}t} = \nabla \cdot \vec{\tau} - \nabla P + \rho g \tag{1}$$

Eq. (2) is obtained by further expansion.

$$\rho \left(\frac{\partial \vec{v}}{\partial t} + \vec{v} \cdot \vec{\nabla} v \right) = \nabla \cdot \vec{\tau} - \nabla P + \rho g \tag{2}$$

where ρ is the fluid density, v is the fluid velocity, t is the time, τ is the stress, P is the pressure, and g is the gravitational acceleration. The left-hand term of the equation is the inertia term, reflecting the increment of fluid momentum per unit volume in unit time. In the parentheses in Eq. (2), there is a dot product of velocity and velocity gradient, which can be expressed as

$$\vec{v} \cdot \vec{\nabla} v = \left| \vec{v} \right| \times \left| \vec{\nabla} v \right| cos\alpha \tag{3}$$

where α is the intersection angle between the velocity gradient and the velocity vector, and can be calculated according to Eq. (4)

$$\alpha = arccos \left(\frac{\vec{v} \cdot \vec{\nabla} v}{\left| \vec{v} \right| \left| \vec{\nabla} v \right|} \right) \tag{4}$$

Here defines the synergy angle α to represent the synergy between the velocity and the velocity gradient. In the range 0°–90°, the dot product Eq. (3) increases with decreasing α, which leads to the increase in momentum and enhancement of mass transfer. This means the interaction of velocity and velocity gradient has an effect on the momentum of the system, that is, the increment of momentum depends not only on the magnitudes of velocity or velocity gradient, but also on the overall synergy between velocity and velocity gradient.

When the synergy angle α becomes zero, the flow is a pure elongational one, and if it becomes 90°, the flow is a pure shear one. Most notably, it is generally known that the effect of elongational flow on mixing is more strong than that of shear flow [19–24], which provides evidence for the feasibility of field synergy analysis. Therefore, the synergy relationship provides a new perspective to understand the polymer mixing.

From Eqs. (2) and (3), we can also conclude that the pressure gradient is affected by the synergy angle α when the stress and gravity terms are invariable. In other words, the synergistic effect of velocity and velocity gradient can reduce

pressure loss and energy consumption, which is of great significance in Newtonian fluid flow. However, for most polymers, which are non-Newtonian in nature, the pressure term has little effect on mechanical power and energy consumption due to its very high viscosity.

2.2 Synergy between velocity and temperature gradient

Almost all polymer processing unit operations require heat transfer processes such as energy exchange, heating, and cooling to facilitate phase-to-phase thermal and molecular mobility. Therefore, the study of energy balance and distribution has special significance in the process of melt flow. It is well known that the general energy conservation equation in the flow field can be represented in the form of Eq. (5).

$$\rho C_V \frac{\mathrm{D}T}{\mathrm{D}t} = -\nabla\cdot \vec{q} \; -T\left(\frac{\partial P}{\partial T}\right)_P \left(\nabla\cdot \vec{v}\right) + \left(\vec{\tau} \; :\nabla\cdot \vec{v}\right) \tag{5}$$

By further expansion, we obtain Eq. (6) as follows.

$$\rho C_V \left(\frac{\partial T}{\partial t} + \vec{v} \cdot \vec{\nabla T}\right) = -\nabla \cdot \left(-K \; \vec{\nabla T}\right) - T\left(\frac{\partial P}{\partial T}\right)_P \left(\nabla\cdot \vec{v}\right) + \left(\vec{\tau} \; :\nabla\cdot \vec{v}\right) \tag{6}$$

where ρ is the fluid density, C_V is the constant-volume specific heat, T is the fluid temperature, v is the fluid velocity, t is the time, τ is the stress, P is the pressure, and K is the heat transfer coefficient. The left-hand term of the equation is the changing rate of internal energy, reflecting the change of heat caused by the temperature variation per unit time at a point in the flow field. Moreover, in the parentheses, there is also a dot product of velocity and temperature gradient. The latter term signifies the interaction between velocity and temperature gradient, and demonstrates that this interaction parameter has an effect on the thermal energy of the system, that is, the change of internal energy depends not only on the velocity field and temperature gradient field, but also on the overall synergy between the velocity field and the temperature gradient field. The dot product in the parentheses in Eq. (6) can be further expressed as

$$\vec{v} \cdot \vec{\nabla T} = \left|\vec{v}\right| \times \left|\vec{\nabla T}\right| cos\beta \tag{7}$$

where β is the intersection angle between the temperature gradient and the velocity vector, and can be calculated according to Eq. (8)

$$\beta = arccos\left(\frac{\vec{v} \cdot \vec{\nabla T}}{\left|\vec{v}\right|\left|\vec{\nabla T}\right|}\right) \tag{8}$$

Here is defined as the synergy angle $\alpha\,\beta$ representing the synergy between the velocity and the temperature gradient. In the range 0°–90°, the dot product (Eq. (7)) increases with decreasing β. When the viscous dissipation power is constant, a small β contributes to a large heat transfer coefficient K, which leads to enhanced heat transfer and temperature uniformity.

In the case of the problem of a two-dimensional flat-plate steady-state boundary layer, Guo et al. [25, 26] have simplified the energy conservation equations into the dimensionless forms

$$Nu_l = \mathrm{Re}_l Pr_l \int_0^{\delta_t,\ lh} \left(\overline{U} \cdot \overline{\nabla T}\right) d\overline{y} \tag{9}$$

where $\overline{U}$ is the velocity vector, $\overline{\nabla T}$ is the temperature gradient vector, Re_l is the l-component of the Reynolds number, Pr_l is the l-component of the Prandtl number, and Nu_l is the l-component of the Nusselt number. Re_l, Pr_l, and Nu_l are expressed as

$$\mathrm{Re}_l = \frac{\rho v \delta_t}{\mu},\ Pr_l = \frac{C_p \mu}{\lambda},\ Nu_l = \frac{K \delta_t}{\lambda} \tag{10}$$

where μ is the fluid viscosity, C_p is the specific heat capacity at constant pressure, λ is the thermal conductivity, and δ_t is the characteristic dimension, which refers to the thickness of the thermal boundary layer. From Eqs. (9) and (10), we can notice that an increase in interaction between the temperature gradient and the velocity fields increases the Nusselt number and the coefficient of local heat transfer, and consequently enhances the overall heat transfer. These synergy equations suggest a new approach to enhance heat transfer of the polymers with poor heat conductivity, namely by increasing the dot product in the integral (Eq. 9).

3. Model design and description

By understanding the multi-field synergy effect in the heat and mass transfer process of polymer plasticization, we can construct a specific flow field so that the directions of velocity field and temperature gradient field are no longer perpendicular, and the flow field movement is more random. The schematic diagram is shown in **Figure 1**. In this way, it can facilitate phase-to-phase thermal and molecular mobility, so as to significantly improve heat transfer and molecular mixing, particularly for highly viscous multicomponent polymer melts with Bio or Nano filler. Based on this method, we can design a special screw configuration to divert the fluid particles and obtain the desired flow field. Here, we propose a new type of screw element, namely, torsion element, to stimulate the spiral or torsional flow, which is the most common way of disturbing or changing flow direction in nature.

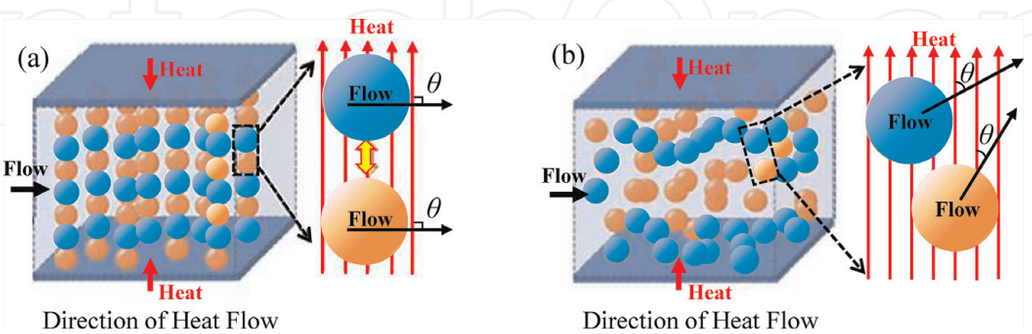

Figure 1.
The synergy between velocity field and heat flow field: Parallel movement (a) and spiral movement (b).

4. Numerical analysis examples

In the following sections, we develop a novel torsion element-induced torsional flow into the flow field by adapting the field synergy principle. Then, we establish a three-dimensional physical and mathematical model with finite element method

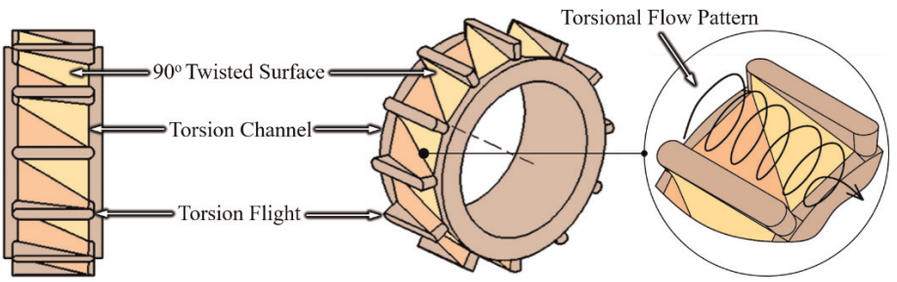

Figure 2.
The geometrical configuration and flow line of particles for a torsion element.

(FEM), and present results of computational fluid dynamics (CFD) simulations of the flow and heat transfer of a viscous polypropylene (PP) melt in the screw with torsion elements to confirm this field synergy method and compared them with the conventional screw in common use today.

The geometrical configuration of the proposed torsion element is shown in **Figure 2**. The torsion channels are divided into N parts along the circumferential direction by torsion flights. Between every two adjacent torsion flights, there are two surfaces twisted by 90°along the axial direction. When polymer flows over the torsion channel, it is expected to undergo a torsional rotation (tumbling) under the forces generated from viscous friction with barrel wall and with the steering between two 90° twisted surfaces. As a result, spiral-shaped or torsional-shaped flow may occur in the torsion channel. In consequence, the intersection angle between the velocity and the heat flux will decrease to less than 90° compared with that in the standard screw channel, and then the synergic effect between the velocity vector and the temperature gradient will be improved.

4.1 Geometrical configuration

Six screws with same length and diameter (designated by alphabetical A to F as shown in **Figure 3**) were employed in this work to verify the synergic effect of

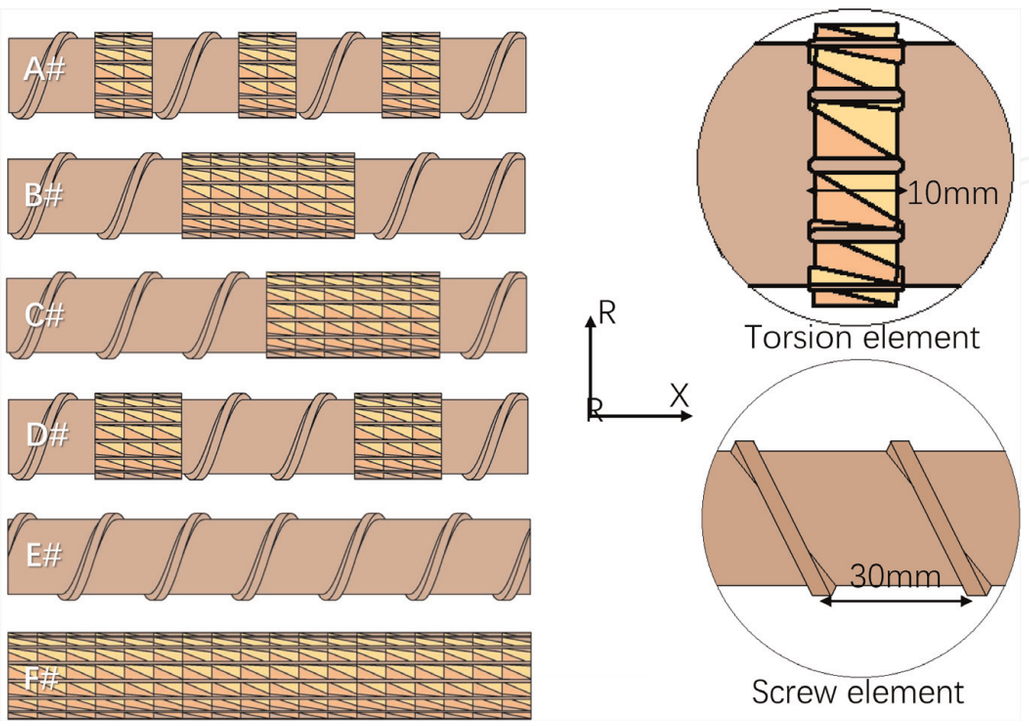

Figure 3.
The geometrical configuration of various screws (with screw elements and torsion elements).

Parameters	Dimensions (mm)
Length of screw	180
Diameter of screw	30
Diameter of barrel	30.4
Length of single torsion element	10
Lead of screw element	30
Inner diameter of screw	25.8

Table 1.
Geometric parameters of simulation models.

torsion element. Screws were constructed of two kinds of polymer plasticization elements: the torsion element and the screw element. Screws A to D had six torsion elements with regular arrangement in different orders. As control subjects, screw E is a conventional screw without torsion element and screw F is a torsional screw without screw elements. **Table 1** presents a summary of the geometric parameters of simulation models.

4.2 Governing equations and boundary conditions

In this case, we assumed that the polymer fluid had non-isothermal transient laminar flow and was incompressible. No-slip conditions were adopted at the boundary. Polypropylene (PP) was chosen to be the model polymer due to its common use in polymer processing. Compared with viscous force, the inertial force can be neglected due to the high viscosity of PP. Therefore, the governing equations representing the flow field in this situation are shown in the form of Eqs. (11)–(13).

Continuity equation:

$$\frac{\partial u_{\mathrm{i}}}{\partial x_{\mathrm{i}}} = 0 \tag{11}$$

Momentum equation:

$$\rho \frac{\partial u_{\mathrm{i}}}{\partial t} + \frac{\partial P}{\partial x_{\mathrm{i}}} = \frac{\partial}{\partial x_{\mathrm{j}}} \left(\eta \frac{\partial u_{\mathrm{i}}}{\partial x_{\mathrm{j}}} \right) \tag{12}$$

Energy equation:

$$\rho c_{\mathrm{p}} \left(\frac{\partial T}{\partial t} + u_{\mathrm{i}} \frac{\partial T}{\partial x_{\mathrm{i}}} \right) = \lambda \frac{\partial^2 T}{\partial x_{\mathrm{i}}^2} + \varphi \tag{13}$$

The apparent viscosity of PP was described by the Carreau-approximate Arrhenius model (Eq. 14), which match most polymers, to consider the factors of both temperature and shear.

$$\eta = \eta_0 \left(1 + t^2 \dot{\gamma}^2\right)^{(n-1)/2} exp\ [-B(T - T_0)] \tag{14}$$

The physical characteristics of the PP and screw material are listed in **Tables 2** and **3**, respectively. The choice of the polymer affects only the constants in the constitutive equation (Eq. (14)). Moreover, the Carreau-approximate Arrhenius model has been already validated for most polymer melts (e.g., polystyrene,

polyethylene, and polyurethane.). Therefore, we assume modeling and simulated results based on the above conditions, which are generally applicable for most of the materials used in polymer processing.

In our work, ANSYS Polyflow 17.0 packaged software (ANSYS, Inc.) was adopted in the simulations. The 3D mesh systems for the screw and the fluid were created using the mesh superposition technique (MST). **Figure 4** shows the 3D model for screw E. The fluid model and screw model were implemented through mesh refinement by hexahedral and tetrahedral elements, respectively. In addition,

Density ρ	735 kg/m^3
Thermal conductivity λ	0.15 W/(m·K)
Specific heat capacity C_p	2100 J/(kg·K)
Zero shear viscosity η_0	26,470 Pa·s
Non-Newtonian index n	0.38
Natural time t	2.15 s
Coefficient of temperature sensibility B	0.02 K^{-1}
Reference temperature T_0	513 K

Table 2.
Physical parameters of the PP.

Density ρ	8030 kg/m^3
Thermal conductivity λ	16.27 W/(m·K)
Specific heat capacity C_p	502.4 J/(kg·K)

Table 3.
Physical parameters of the screw.

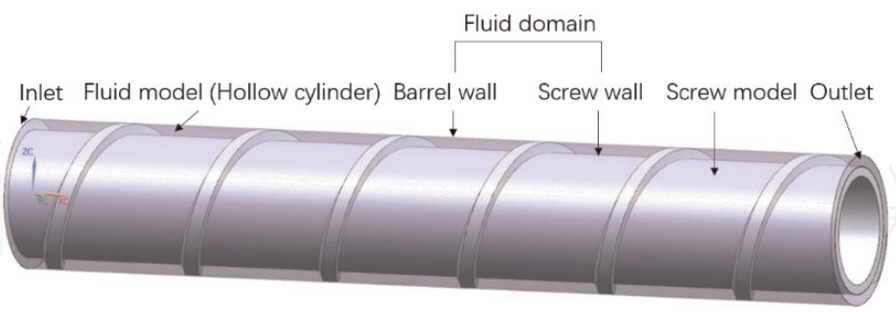

Figure 4.
Three-dimensional physical model of screw E.

Location	Flow boundary conditions	Thermal boundary conditions
Inlet	Setting zero pressure	513 K
Outlet	Setting zero pressure	Heat outlet
Barrel wall	No-slip wall	513 K
Screw wall	Screw speeds: 40,60,80,100,120 r/min	Free boundary

Table 4.
Boundary conditions.

progressively refined meshes for the screw and fluid models were constructed to ensure that the simulation results were mesh-independent. Different screws had the same mesh refinement setting and, with the same fluid model, simulation results were displayed in the grid of fluid domain. **Table 4** gives the flow and thermal boundary conditions used in this case.

5. Results and discussion

5.1 Temperature uniformity

Firstly, we investigated the axial melt temperature distribution by selecting different radial reference lines for these six screws as shown in **Figure 5**. From all the six screws, we can find that the temperature fluctuations decrease by the effect of torsion elements and the temperature difference between melt and barrel wall in the position of torsion elements is smaller than that of the position of screw elements. The reason for this phenomenon is heat transfer enhancement caused by the synergy effect between velocity and temperature gradient. We will prove this in the next section. **Figure 6** shows the radial melt temperature distribution for screw B in the position of torsion and screw elements. For the position of torsion element, almost all the fluid is in a high-temperature region, more than 500°C, while the radial temperature for most fluid in the screw channels is below 500°C. Results indicated that the radial temperature difference in the position of torsion element is much lower compared with that of the position of screw elements, no matter before

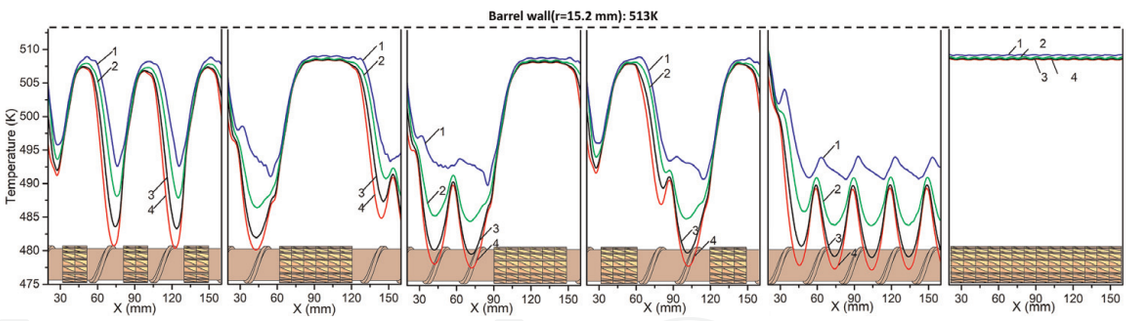

Figure 5.
Radial and axial temperature distribution for the different screws at 40 r/min. (1) r = 14.5 mm; (2) r = 14.0 mm; (3) r = 13.5 mm; (4) r = 13.0 mm.

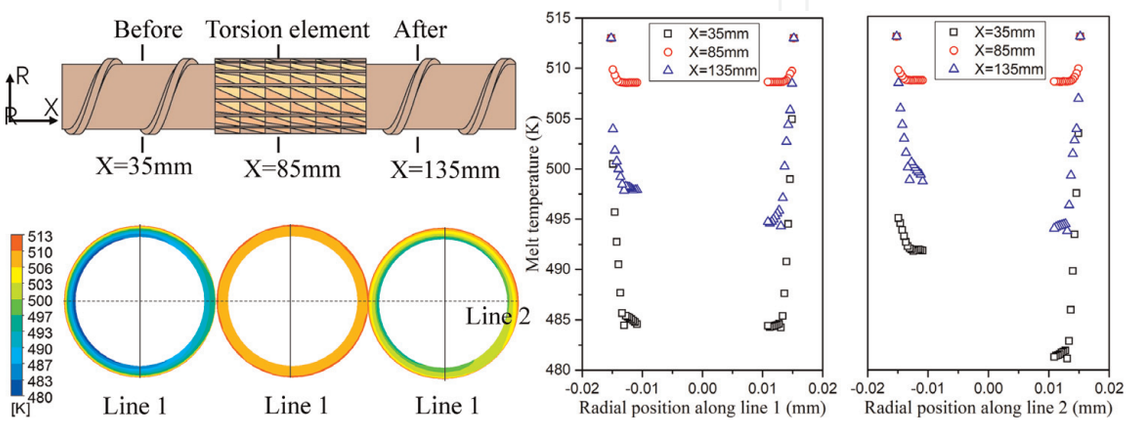

Figure 6.
Temperature contours (left) and melt temperature profiles (right) across the melt flow with the magnitude of fluctuations for screw B at different x-positions at 40 r/min.

or after the torsion element. It can be concluded that the torsion element can achieve more uniform temperature distribution than the screw element.

5.2 Field synergy analysis

In order to verify the field synergy effect, we calculated the mean field synergy angle between temperature gradient and velocity fields and the Nusselt number at different screw speeds for these six screws as shown in **Figure 7**. It can be seen that the Nusselt number increases with screw speed, which is a well-known fact. Results also indicated that conventional screw E without torsion elements has the largest mean field synergy angle and smallest Nusselt number, while screw F without screw elements has the smallest mean field synergy angle and largest Nusselt number, which means the smaller the field synergy angle, the larger the Nusselt number. However, there are little difference of values in field synergy angle and Nusselt number for the screws A, B, C and D. This is because all these four screws have the same six torsion elements, which bring about almost the same influence on the variations of field synergy angle, that is, the arrangement of torsion elements in the screw has little effect on the field synergy angle. Therefore, it can be inferred that the screws equipped with torsion elements show better convective heat transfer capacity compared with the conventional screw, which then bring about a good melt temperature uniformity.

In addition, **Figure 8** shows the local field synergy angle and the local heat transfer coefficient at different cross sections for screw A. Results also indicated that the local regions with torsion elements have larger heat transfer coefficients and smaller field synergy angles than the local regions with screw elements. Besides, the local convective heat transfer was found to be inversely proportional to the local field synergy angle between velocity and temperature gradient.

The contours of the local field synergy angle at different positions further show that most of the local synergy angle distributions at the cross sections of torsion elements alternate between larger and smaller synergy angles, while those at the cross sections of screw elements are close to 90.0°.

Figure 9 shows the dependence of the Nusselt number on the field synergy angle for various screw speeds and shows that the Nusselt number increases with

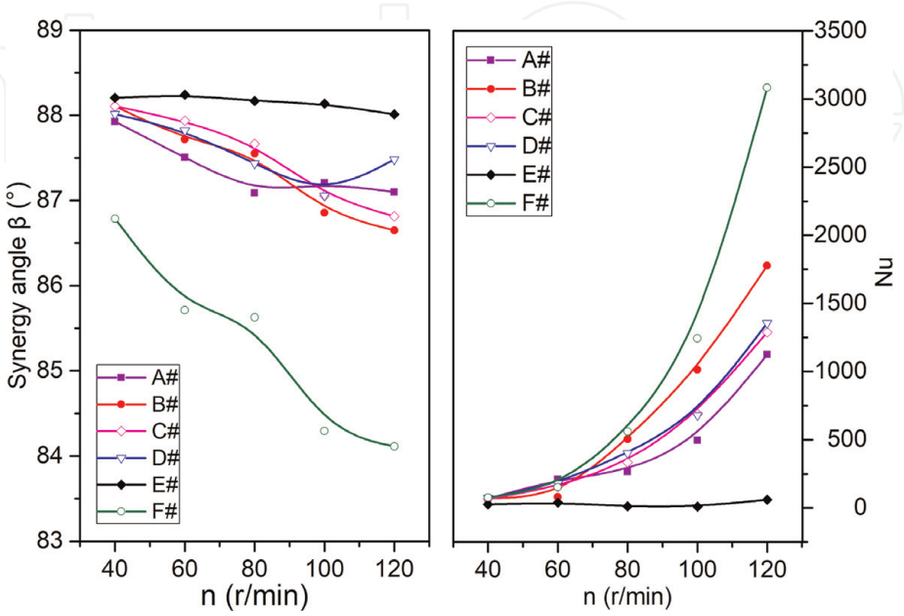

Figure 7.
A plot of the mean field synergy angle (left) and Nusselt number (right) versus screw speed for various screws.

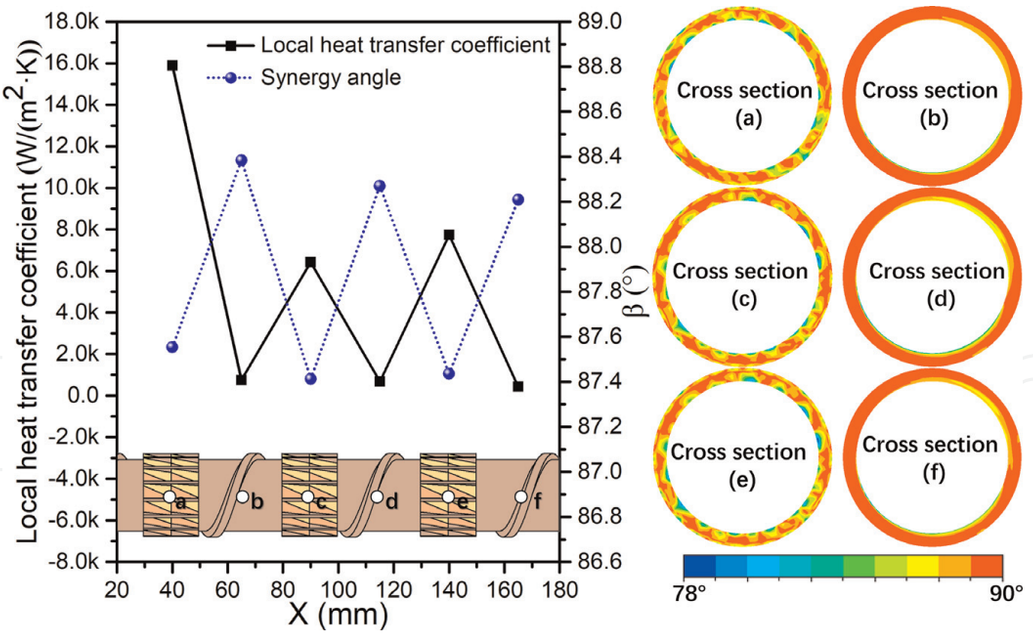

Figure 8.
A plot of the local field synergy angle versus the local heat transfer coefficient (left) and the local field synergy angle contours at different cross sections (right) for screw A at a screw speed of 80 r/min.

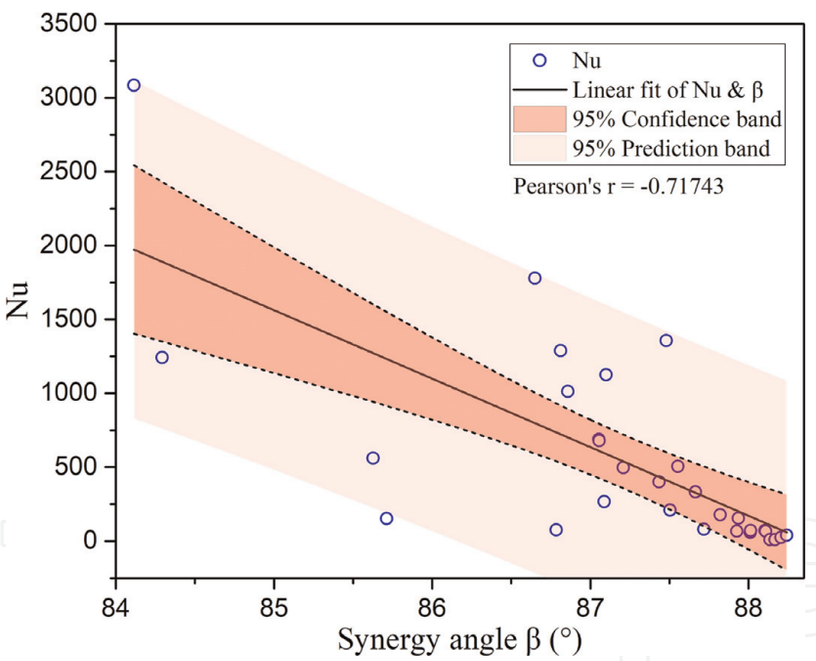

Figure 9.
The dependence of the Nusselt number on the field synergy angle for various screw speeds. The inset is the Pearson correlation coefficient.

decreasing field synergy angle. It can be inferred that the Nusselt number is inversely interrelated with the synergy angle β. When the confidence level is 95%, its value is limited to a relatively narrow confidence band. Furthermore, the Pearson correlation coefficient is about −0.7, which indicates a strong negative correlation. These results demonstrate that the coupling relationship between temperature gradient and velocity fields has a significant effect on the convective heat transfer of the polymer itself in a polymer plasticization process.

Accordingly, the field synergy principle is able to explain the enhancement of heat transfer brought about by the torsion elements.

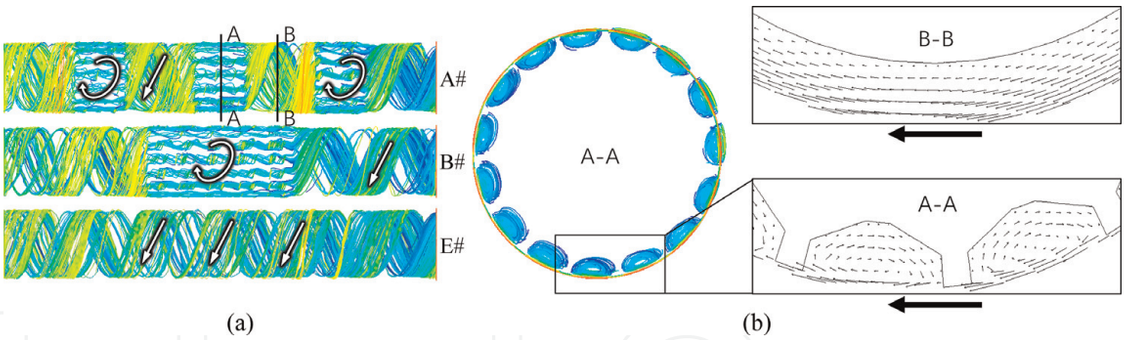

Figure 10.
The streamline contours in screws A, B, and E at a screw speed of 40 r/min in the axial direction (a) and the cross section of the torsion element (b).

5.3 Fluid flow behavior

As stated previously, the synergy effect between velocity and temperature gradient in the torsion element is realized by constructing a spiral or torsional flow in the flow field. In order to verify the existence of torsional-spiral shaped flow, we investigated the fluid flow characteristics in the region of both torsion and screw elements as shown in **Figure 10**.

Figure 10(a) shows the streamline contours along the axial direction for screws A, B, and E. We can see that spiral-shaped flow occurs in the position of torsion elements for both screws A and B, which cannot be achieved in screw E. In this spiral-shaped flow, the velocity directions are changing along the flow direction and mass transfer is enhanced in the radial direction, that is, the synergy angles between velocity and thermal flow fields are no longer perpendicular to each other, which confirms the assumption shown in **Figures 1** and **2**. **Figure 10(b)** shows the cross sections in the torsion and screw elements. And results indicated that there are vortexes in the torsion channel, while there are just plug flows without radial convection in the screw channel.

Therefore, it can be inferred that the torsion element improves the synergy between velocity and temperature gradient by inducing torsional flow, and then enhances heat transfer in the screw plasticization process.

6. Experimental validation

The performance of screw with torsion elements in the polymer plasticization process has been verified though numerical analysis. Furthermore, the mixing and heat transfer performances of the newly designed screw configuration based on field synergy principle were evaluated through extrusion runs and experimental data. Materials used were polypropylene (PP) and polystyrene (PS) bi-phase polymer composite mix.

Figure 11 shows the particle size distribution of PS (PP: PS = 100:10, % wt/wt) at the screw outlet; more specifically, **Figure 11(a)** is that of torsional screw with six torsion elements and **Figure 11(b)** is that of conventional screw without torsion element. The particle size distribution of PS fits Gaussian distribution. On the other hand, the relative frequencies of particle size in torsion screw are more concentrated in a narrow range [0–50 μm] than those in conventional screw. This can be further validated from the scanning electron microscope (SEM) pictures shown in **Figure 11(a)** and **Figure 11(b)**. SEM pictures clearly show that the particles of PS in torsional screw are finer and the particle sizes are smaller than those in conventional

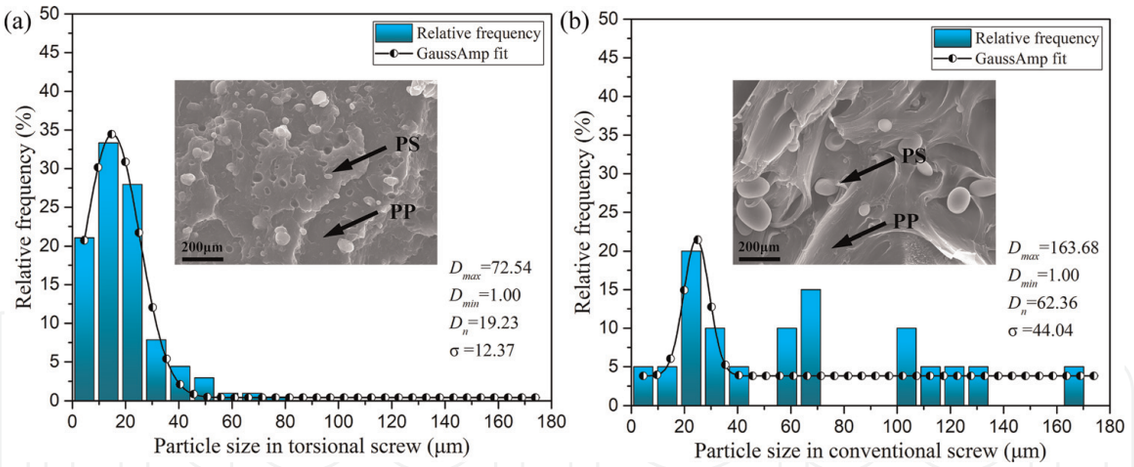

Figure 11.
Particle size distribution in a PP/PS bi-phase composite in the outlet of the screws.

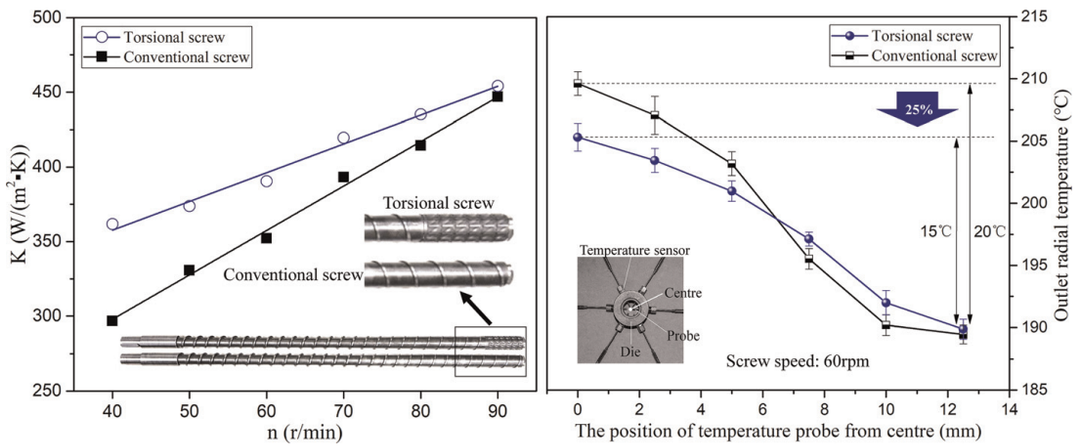

Figure 12.
Heat transfer coefficient (left) and outlet radial temperature distribution (right) of the plasticization system for screws.

screw. Average particle size (*Dn*), the maximum value, minimum value, and standard deviation of particle size of PS are also calculated and summarized in **Figure 11**. Results indicate that the *Dn*, the standard deviation, and maximum value of particle size in torsional screw are much smaller than those in conventional screw. Therefore, the torsional screw with six torsion elements shows good mixing performance.

Figure 12 shows the variation of heat transfer coefficient *K* with screw speed and the outlet radial temperature distribution at 60 r/min for torsional screw and conventional screw. From the heat transfer coefficient *K*, we can see that the *K* value improves with screw speed, which is in agreement with **Figure 7**. More interestingly, the *K* value for torsional screw is higher than that for conventional screw, indicating that the torsional screw with six torsion elements shows better heat transfer capability than that of the conventional screw. Therefore, we can confirm that the configuration of torsion element designed based on field synergy principle can in fact enhance heat transfer, which is in agreement with the simulation results.

From the outlet radial temperature distribution, it can be found that the melt temperature in the center of die is higher than the temperature near the barrel walls, which is due to the viscous dissipation of polymers. Therefore, an effective heat transfer is needed in order to evenly distribute the thermal energy among the

polymer melt. In addition, the radial temperature difference of torsional screw is 15° C, whereas the radial temperature difference of conventional screw is 20°C, which is 25% higher than that of torsional screw. As the experiment data indicate that the radial temperature difference of melt decreases in the torsional configured screw, it can be concluded that the torsional configuration has a superior heat and mass transfer performance to achieve better temperature distribution than traditional screw, which is also in agreement with the simulation results.

7. Conclusions

One of the fundamental questions of non-uniform heat and mass transfer in viscous fluid was addressed by proposing a radial torsional flow pattern, by designing a torsion element and validating the same in a melt-phase polymer extrusion process. The synergistic interaction mechanisms between velocity and velocity gradient and velocity and temperature gradient have been investigated by considering theoretical and numerical aspects, which provides a new perspective to understand the polymer processing. Considering the multi-field synergy, a new design concept of torsion screw configuration has been proposed to facilitate phase-to-phase thermal and molecular mobility.

The spiral-shaped torsional flow induced by torsion configurations in a polymer channel changes the radial velocity direction, which in turn improves the interaction between velocity and temperature fields and helps to achieve good heat transfer and temperature homogeneity. The new torsion elements and their arrangement provide a novel pathway to achieve good thermal management of polymer melt by enhancing multi-field coupling. These results can be achieved to guide the screw design used for preparing high-performance composites, especially heat-sensible and biodegradable nanocomposites or microcellular foam controlled by temperature.

Acknowledgements

This work was supported by the National Natural Science Foundation of China (grant number 51576012). Support from China Scholarship Council is also gratefully acknowledged for Ranran Jian's joint PhD grant.

Appendices and Nomenclature

ρ	fluid density, kg/m^3
v	fluid velocity, m/s
τ	stress, Pa
P	pressure, Pa
C_V	constant-volume specific heat capacity, J/(kg·K)
C_p	constant-pressure specific heat capacity, J/(kg·K)
λ	thermal conductivity, W/(m·K)
T	fluid temperature, K
x, y, z	Cartesian coordinates, m
δ	velocity boundary layer thickness, m

δ_t	thermal boundary layer thickness, m
$\overline{U}$	velocity vector, m/s
$\overline{\nabla U}$	velocity gradient vector, s^{-1}
$\overline{\nabla T}$	temperature gradient vector, K/m
v_m	mean velocity of fluid, m/s
μ	fluid viscosity, Pa·s
K	heat transfer coefficient, W/(m2·K)
Re	Reynolds number
Eu	Euler number
Pr	Prandtl number
Nu	Nusselt number
α	synergy angle between the velocity gradient and the velocity, °
β	synergy angle between the temperature gradient and the velocity, °
P	pressure, Pa
η	apparent viscosity, Pa·s
η_0	zero shear viscosity, Pa·s
$\dot{\gamma}$	shear rate, s^{-1}
t	natural time, s
B	temperature sensibility coefficient, K^{-1}
n	non-Newtonian index
T_0	reference temperature, K

Author details

Ranran Jian[1,2], Hongbo Chen[3] and Weimin Yang[1*]

1 College of Mechanical and Electrical Engineering, Beijing University of Chemical Technology, Beijing, China

2 Centre for Biocomposites and Biomaterial Processing, Department of Mechanical and Industrial Engineering, University of Toronto, Toronto, ON, Canada

3 College of Electromechanical Engineering, Qingdao University of Science and Technology, Qingdao, China

*Address all correspondence to: yangwmr@gmail.com

References

[1] Deng J, Li K, Harkin-Jones E, Price M, Karnachi N, Kelly A, et al. Energy monitoring and quality control of a single screw extruder. Applied Energy. 2014;**113**:1775-1785

[2] Abeykoon C, Martin PJ, Kelly AL, Li K, Brown EC, Coates PD. Investigation of the temperature homogeneity of die melt flows in polymer extrusion. Polymer Engineering and Science. 2014;**54**(10): 2430-2440

[3] Tong FH, Shi DL, Qin JH. Single screw extruder characteristics on friction and heat generated with the barrel carved spiral groove. In: Wang CH, Ma LX, Yang W, editors. Advanced Polymer Science and Engineering. Stafa-Zurich: Trans Tech Publications Ltd; 2011. pp. 668-673

[4] Rauwendaal C. New developments in mixing and screw design. Plastics, Additives and Compounding. 2008; **10**(6):32-36

[5] Rauwendaal C. New screw design for cooling extruders. Plastics, Rubber and Composites. 2004;**33**(9–10):397-399

[6] Kelly AL, Brown EC, Coates PD. The effect of screw geometry on melt temperature profile in single screw extrusion. Polymer Engineering And Science. 2006;**46**(12):1706-1714

[7] Huang MS. Design analysis of a standard injection screw for plasticising polycarbonate resins. Journal of Polymer Engineering. 2016;**36**(5): 537-548

[8] Abeykoon C, Kelly AL, Brown EC, Coates PD. The effect of materials, process settings and screw geometry on energy consumption and melt temperature in single screw extrusion. Applied Energy. 2016;**180**:880-894

[9] Spalding MA, Kuhman JA, Kuhman J, Prettyman L, Larson D. Performance of a distributive melt-mixing screw with an advanced mixing tip. In: Antec-Conference Proceedings. Chicago; 2004. pp. 599-604

[10] Shimbo M, Nishida K, Heraku T, Iijima K, Sekino T, Terayama T, et al. Foam Processing Technology of Microcellular Plastics by Injection Mold Machine. Brookfield Center: Soc Plastics Engineers; 1999

[11] Potente H, Stenzel H. Computational design of spiral shearing sections. Kunststoffe-German Plastics. 1991; **81**(2):153-156

[12] Zitzenbacher G, Karlbauer R, Thiel H. A new calculation model and optimization method for Maddock mixers in single screw plasticising technology. International Polymer Processing. 2007;**22**(1):73-81

[13] Rydzkowski T. Plasticization degree of extrudate obtained during autothermal work of screw-disc extruder. Polymers. 2009;**54**(5):377-381

[14] Qu JP, Zhao XQ, Li JB. Power consumption analysis of polymer solids discharging process in vane plasticization extruder. In: Chen WZ, Xu XP, Dai PQ, Chen YL, editors. Advanced Manufacturing Technology, Pts 1–4. Stafa-Zurich: Trans Tech Publications Ltd; 2012. pp. 1941-1944

[15] Qu JP, Yang ZT, Yin XC, He HZ, Feng YH. Characteristics study of polymer melt conveying capacity in vane plasticization extruder. Polymer-Plastics Technology and Engineering. 2009;**48**(12):1269-1274

[16] Diekmann C. Direct-drive singlescrew extruders. Kunststoffe-Plast Europe. 2004;**94**(9):243-245

[17] Jiang BY, Peng HJ, Wu WQ, Jia YL, Zhang YP. Numerical Simulation and experimental investigation of the viscoelastic heating mechanism in ultrasonic plasticizing of amorphous polymers for micro injection molding. Polymers. 2016;**8**(5):199

[18] Jinping Q, Baiping X, Gang J, Hezhi H, Xiangfang P. Performance of filled polymer systems under novel dynamic extrusion processing conditions. Plastics, Rubber and Composites. 2002;**31**(10):432-435

[19] Yin XC, Li S, He GJ, Zhang GZ, Qu JP. Experimental study of the extrusion characteristic of a vane extruder based on extensional flow. Advances in Polymer Technology. 2016; **35**(2):215-220

[20] Wen JS, Liang YH, Chen ZM. Numerical simulation of elongational flow in polymer vane extruder. In: Jiang ZY, Han JT, Liu XH, editors. Advanced Design Technology. Stafa-Zurich: Trans Tech Publications Ltd; 2012. pp. 415-418

[21] Ragoubi M, Zouari R, Ben Abdeljawad M, Terrie C, Baffoun A, Alix S, et al. Design of doum palm fibers biocomposites by reactor/elongational flow MiXer: Evaluation of morphological, mechanical, and microstructural performances. Polymer Composites. 2018;**39**:519-530

[22] Pierrot FX, Ibarra-Gomez R, Bouquey M, Muller R, Serra CA. In situ polymerization of styrene into a PMMA matrix by using an extensional flow mixing device: A new experimental approach to elaborate polymer blends. Polymer. 2017;**109**:160-169

[23] Cao CL, Chen XC, Wang JX, Lin Y, Guo YY, Qian QR, et al. Structure and properties of ultrahigh molecular weight polyethylene processed under a consecutive elongational flow. Journal of Polymer Research. 2017;**25**(1):16

[24] Bouquey M, Loux C, Muller R, Bouchet G. Morphological study of two-phase polymer blends during compounding in a novel compounder on the basis of elongational flows. Journal of Applied Polymer Science. 2011; **119**(1):482-490

[25] Guo ZY, Li DY, Wang BX. A novel concept for convective heat transfer enhancement. International Journal of Heat and Mass Transfer. 1998;**41**(14): 2221-2225

[26] Guo ZY, Tao WQ, Shah RK. The field synergy (coordination) principle and its applications in enhancing single phase convective heat transfer. International Journal of Heat and Mass Transfer. 2005;**48**(9):1797-1807